Physics Letters A 541 (2025) 130407

Contents lists available at ScienceDirect

Physics Letters A

journal homepage: www.elsevier.com/locate/pla

Letter

Optical characteristics of Bessel-Gaussian beams

M. Alquraishi [a,*], V.E. Lembessis [b]

[a] Department of Computer Science, College of Engineering and Information Technology, Onaizah Colleges, Qassim, Saudi Arabia
[b] Photonics Group, Department of Physics and Astronomy, College of Science, King Saud University, Riyadh 11451, Saudi Arabia

ARTICLE INFO

Communicated by S. Khonina

ABSTRACT

A physically realizable set of optical Bessel beams is identified as the Bessel-Gaussian (BG) mode, which can be obtained by modulating the radial oscillations of the Bessel beams with a Gaussian profile. The BG type mode can possess orbital angular momentum as well as optical spin. We explore the optical properties of the BG modes for a fixed power, particularly their spin and angular momenta, energy, and helicity. The findings are compared to those of the Truncated Optical Bessel (TOB) modes and the Laguerre-Gaussian (LG) modes.

1. Introduction

Bessel beams [1,2] are well-known as ideal solutions to the vector Helmholtz equation in cylindrical coordinates. Such beams can be endowed with orbital angular momentum (OAM) as well as spin angular momentum (SAM). They propagate over a large distance in free-space without changing their transverse shape, giving rise to a non-diffractive property. Therefore, the ideal form of such beams would require an infinite amount of energy and, for this reason, cannot be created in practice. Although a small amount of energy is contained within the central lobe of a Bessel beam, compared to diffracting Gaussian beams, large distances can be covered by a Bessel beam than a Gaussian beam of the same spot size, at the expense of the power-transport efficiency [3]. Bessel beams have attracted much attention in both theory and experiment, and their applications cover many areas, including optical trapping and manipulation of tiny particles [4–7], material processing [8], and others [9].

One experimentally realizable form of the Bessel beams with a finite amount of energy is the so-called Bessel-Gaussian (BG) beam [10], which has the form of the ℓth-order Bessel function of the first kind multiplied by a Gaussian profile and a helical phase of the form $e^{i\ell\phi}$, where ℓ is the winding number, also called the 'azimuthal mode number' and ϕ is the azimuthal angle. Several methods to generate a BG beam have been proposed and demonstrated, such as using an annular slit in the back focal plane of a lens [2], or an axicon [11], or a deformable mirror [12], or spatial light modulators (SLMs) [13].

This paper examines the main properties of the BG modes in the sense described in Section 2, namely SAM, angular momentum (AM), energy, and optical helicity. Recent studies have explored these properties for two members of optical vortices: the Truncated Optical Bessel (TOB) beams [14], and the LG beams [15]. In Section 3, we define the cycle-averaged densities, discuss them in turn in the next sections, and find the total respective properties by integrating the corresponding optical densities. Finally, in Section 8, we discuss our conclusions.

2. Bessel-Gaussian beams

For a light beam of the BG form, its electric and magnetic fields can be derived from a transverse vector potential, which, in cylindrical polar coordinates $\mathbf{r} = (\rho, \phi, z)$, takes the form

$$\mathbf{A}_\ell(\mathbf{r}, t) = (\alpha\hat{\mathbf{x}} + \beta\hat{\mathbf{y}})\mathcal{F}_\ell(\rho, \phi)e^{i(k_z z - \omega t)}, \tag{1}$$

where α and β are complex constants, which have the following properties:

$$|\alpha|^2 + |\beta|^2 = 1; \sigma = i\left(\alpha\beta^* - \alpha^*\beta\right). \tag{2}$$

In the case of linearly polarized light, we have $\alpha = 1$ and $\beta = 0$, while in the case of circularly polarized light we have $\alpha = 1/\sqrt{2}$ and $\beta = i/\sqrt{2}$.

The wave number k_z in Eq. (1) stands for the longitudinal wave number of a light beam traveling along the $+z$ direction, which is related to the magnitude of the total wave vector $\mathbf{k}$ by the relation $k = \sqrt{k_z^2 + k_\perp^2}$, ω is the angular frequency, and $\mathcal{F}_\ell(\rho, \phi)$ is the amplitude function of the BG mode of a winding number ℓ which, at $z = 0$, is given by [10]

$$\mathcal{F}_\ell(\rho, \phi) = \frac{\mathcal{E}_0}{\omega} J_{|\ell|}\left(k_\perp \rho\right) e^{-\frac{\rho^2}{w_0^2}} e^{i\ell\phi}, \tag{3}$$

where $J_{|\ell|}$ is the Bessel function of the first kind of order ℓ, $k_\perp$ is the transverse wave number of the beam, w_0 is the beam waist in the focal

* Corresponding author.
E-mail address: qumadhawi@gmail.com (M. Alquraishi).

https://doi.org/10.1016/j.physleta.2025.130407
Received 25 January 2025; Received in revised form 22 February 2025; Accepted 3 March 2025

Available online 5 March 2025

plane $z=0$, and $\mathcal{E}_0$ is an overall normalization factor. The BG beams are characterized by two parameters, namely the beam waist w_0 similar to the case of a standard Laguerre-Gaussian (LG) beam, and the Bessel argument $k_\perp$ which is the in-plane wave number such that $k_\perp = \sqrt{k_x^2 + k_y^2}$. Note that both the Gaussian beam and the Bessel beam can be obtained as special cases by a suitable choice of $k_\perp$ and w_0. The radial oscillatory behavior of the Bessel term dominates with increasing $k_\perp$. The well-known LG beams are characterized by two indices: the azimuthal mode index ℓ and the radial index p. Bessel beams, on the other hand, are only described by the index ℓ and theoretically have an infinite number of concentric rings, such as the standard LG beams with a large number of p. However, in the case of truncated Bessel beams, the index p appears and determines the zero of the Bessel function [14], while in the case of BG beams, the number of rings depends on the choice of the parameters $k_\perp$ and w_0 which can be experimentally realized [16].

The factor $\mathcal{E}_0$ in Eq. (3) is the normalization constant, which is fixed in terms of the applied power $\mathcal{P}$. The derivation of this factor is given in Appendix A, and the final result is:

$$\mathcal{E}_0^2 = \frac{4\mu_0 \mathcal{P}\omega^2}{c\pi k_z^2 w_0^2 e^{-\frac{k_\perp^2 w_0^2}{4}} I_{|\ell|}\left(\frac{k_\perp^2 w_0^2}{4}\right)}, \tag{4}$$

where $I_{|\ell|}$ is the modified Bessel function of the first order ℓ. The normalization factor of a BG mode differs from that of a LG mode, given in Ref. [15], by the existence of the exponential function and the modified Bessel function in the denominator.

The magnetic field of the BG mode can be directly obtained from $\mathbf{B} = \nabla \times \mathbf{A}$ and has the form

$$\mathbf{B} = \left[ik_z(\alpha\hat{\mathbf{y}} - \beta\hat{\mathbf{x}})\mathcal{F} + \left(\beta\frac{\partial\mathcal{F}}{\partial x} - \alpha\frac{\partial\mathcal{F}}{\partial y}\right)\hat{\mathbf{z}}\right] e^{ik_z z}, \tag{5}$$

where for ease of notation we do not show the time exponential function $e^{i\omega t}$ and we drop the label ℓ and the arguments ρ and ϕ in the mode function $\mathcal{F}$. The magnetic field satisfies $\nabla \cdot \mathbf{B} = 0$. In addition to the zeroth-order transverse components, the field also involves the first-order longitudinal (or axial) component. The magnitude of this component is comparable to that of the transverse one when the spot size of the beam is sufficiently small. By using Maxwell's equation $\mathbf{E} = (ic^2/\omega)\nabla \times \mathbf{B}$, the electric field $\mathbf{E}$ follows from the magnetic field $\mathbf{B}$ and can be written as follows

$$\mathbf{E} = c\left[ik_z(\alpha\hat{\mathbf{x}} + \beta\hat{\mathbf{y}})\mathcal{F} - \left(\alpha\frac{\partial\mathcal{F}}{\partial x} + \beta\frac{\partial\mathcal{F}}{\partial y}\right)\hat{\mathbf{z}}\right] \times e^{ik_z z}. \tag{6}$$

This field also includes the zeroth-order transverse components and the first-order longitudinal component. It satisfies $\nabla \cdot \mathbf{E} = 0$. Note that both $\mathbf{E}$ and $\mathbf{B}$ satisfy duality using Maxwell's equations in the sense that we can derive the field $\mathbf{E}$ from $\mathbf{B}$, and vice versa.

3. Cycle-averaged optical properties

In this section, we summarize the main properties: the SAM density $\bar{\mathbf{s}}$, the Poynting vector $\bar{\mathbf{w}}$, the linear momentum density $\bar{\pi}$, the angular momentum (AM) density $\bar{\mathbf{j}}$, and the cycle-averaged helicity density $\bar{\eta}$, which, respectively, are defined as follows

$$\bar{\mathbf{s}} = \frac{\epsilon_0}{2\omega}\Im\left[\mathbf{E}^* \times \mathbf{E}\right], \tag{7}$$

$$\bar{\mathbf{w}} = \frac{1}{2\mu_0}\Re\left[\mathbf{E}^* \times \mathbf{B}\right], \tag{8}$$

$$\bar{\pi} = \frac{\bar{\mathbf{w}}}{c^2}, \tag{9}$$

$$\bar{\mathbf{j}} = \mathbf{r} \times \bar{\pi}, \tag{10}$$

$$\bar{\eta}(\mathbf{r}) = -\frac{\epsilon_0 c}{2\omega}\Im\left[\mathbf{E}^* \cdot \mathbf{B}\right], \tag{11}$$

where $\Im[\ldots]$ and $\Re[\ldots]$ stand for the imaginary and real part of $[\ldots]$, respectively, and the superscript $*$ stands for the complex conjugate.

As outlined previously, we evaluate in turn the densities given above using the expressions of the magnetic and electric fields, given by Eqs. (5) and (6) with regard to the BG beams.

4. SAM density of BG beams

The cycle-averaged SAM density, given by Eq. (7), can be directly evaluated using Eq. (6). The transverse SAM components are obtained as follows

$$\begin{aligned}\bar{s}_x &= \frac{\epsilon_0}{2\omega}\Im\left[\mathbf{E}^* \times \mathbf{E}\right]_x \\ &= -\frac{c^2 k_z \epsilon_0}{2\omega}\left\{\left[\beta^*\alpha\mathcal{F}^*\left(\frac{\partial\mathcal{F}}{\partial x}\right) + \alpha^*\beta\mathcal{F}\left(\frac{\partial\mathcal{F}}{\partial x}\right)^*\right]\right. \\ &\left. + |\beta|^2\left[\mathcal{F}^*\left(\frac{\partial\mathcal{F}}{\partial y}\right) + \mathcal{F}\left(\frac{\partial\mathcal{F}}{\partial y}\right)^*\right]\right\},\end{aligned} \tag{12}$$

and

$$\begin{aligned}\bar{s}_y &= \frac{\epsilon_0}{2\omega}\Im\left[\mathbf{E}^* \times \mathbf{E}\right]_y \\ &= -\frac{c^2 k_z \epsilon_0}{2\omega}\left\{\left[\alpha\beta^*\mathcal{F}\left(\frac{\partial\mathcal{F}}{\partial y}\right)^* + \alpha^*\beta\mathcal{F}^*\left(\frac{\partial\mathcal{F}}{\partial y}\right)\right]\right. \\ &\left. + |\alpha|^2\left[\mathcal{F}\left(\frac{\partial\mathcal{F}}{\partial x}\right)^* + \mathcal{F}^*\left(\frac{\partial\mathcal{F}}{\partial x}\right)\right]\right\}.\end{aligned} \tag{13}$$

The x- and y-component derivatives of $\mathcal{F}$ in Eqs. (12) and (13) are as follows

$$\left(\frac{\partial\mathcal{F}}{\partial x}\right) = (\mathcal{D}\cos\phi - i\mathcal{T}\sin\phi)\mathcal{F}, \tag{14}$$

and

$$\left(\frac{\partial\mathcal{F}}{\partial y}\right) = (\mathcal{D}\sin\phi + i\mathcal{T}\cos\phi)\mathcal{F}, \tag{15}$$

where $\mathcal{D}$ and $\mathcal{T}$, for a general BG mode, are given by

$$\mathcal{D} = \left\{-\frac{2\rho}{w_0^2} + \frac{|\ell|}{\rho} - k_\perp\frac{J_{|\ell|+1}(k_\perp\rho)}{J_{|\ell|}(k_\perp\rho)}\right\}; \mathcal{T} = \frac{\ell}{\rho}. \tag{16}$$

Substituting Eqs. (14) and (15) into Eqs. (12) and (13), and using Eq. (2), we have

$$\bar{s}_x = -\frac{c^2 k_z \epsilon_0}{2\omega}(\sigma\mathcal{T} - \mathcal{D})\sin\phi\,|\mathcal{F}|^2, \tag{17}$$

and

$$\bar{s}_y = -\frac{c^2 k_z \epsilon_0}{2\omega}(\sigma\mathcal{T} - \mathcal{D})\cos\phi\,|\mathcal{F}|^2. \tag{18}$$

The two transverse components involve a spin-orbit $\sigma\ell$ coupling (the first term), and both are non-zero due to the contribution of the first-order longitudinal component. The only difference between them is that $\bar{s}_x$ is proportional to $\sin\phi$, while $\bar{s}_y$ is proportional to $\cos\phi$. However, the integral values of these two components are zero ($\bar{S}_x = 0 = \bar{S}_y$) due to the angular integral, so both components do not contribute to the total spin. Note that for a weakly focused field, we always have $\bar{s}_x = \bar{s}_y = 0$.

On the other hand, the longitudinal SAM component is given by

$$\bar{s}_z = \frac{\epsilon_0}{2\omega}\Im\left[\mathbf{E}^* \times \mathbf{E}\right]_z = \frac{c^2 k_z^2 \epsilon_0}{2\omega}\sigma\,|\mathcal{F}|^2. \tag{19}$$

This equation shows that the longitudinal component of the SAM is σ-dependent and thus is zero for linearly polarized beams ($\sigma = 0$). The only non-vanishing component of the SAM on integration is the z-component, which is given by

$$\bar{S}_z = \frac{\pi\mathcal{E}_0^2 c^2 k_z^2 \epsilon_0}{\omega^3}\sigma\int_0^\infty \left|J_{|\ell|}(k_\perp\rho)\right|^2 e^{-\frac{2\rho^2}{w_0^2}}\rho d\rho. \tag{20}$$

We make use of the following standard integral:

$$\int_0^\infty \left|J_{|\ell|}\left(k_\perp \rho\right)\right|^2 e^{-\frac{2\rho^2}{w_0^2}} \rho d\rho = \frac{w_0^2}{4} e^{-\frac{k_\perp^2 w_0^2}{4}} I_{|\ell|}\left(\frac{k_\perp^2 w_0^2}{4}\right). \tag{21}$$

Then, Eq. (20) becomes

$$\bar{S}_z = \frac{\pi \mathcal{E}_0^2 c^2 k_z^2 \epsilon_0 w_0^2}{4\omega^3} \sigma e^{-\frac{k_\perp^2 w_0^2}{4}} I_{|\ell|}\left(\frac{k_\perp^2 w_0^2}{4}\right). \tag{22}$$

Substituting for $\mathcal{E}_0$, we obtain

$$\bar{S}_z = \sigma\left(\frac{\mathcal{P}}{\omega c}\right) = \sigma L_0, \tag{23}$$

where $L_0 = (\mathcal{P}/\omega c)$ is constant, which has the dimensions of angular momentum per unit length. The same results are also obtained for the total SAM of both LG and TOB modes [14,15].

5. AM and energy of BG beams

The three components of the cycle-averaged Poynting vector $\bar{\mathbf{w}}$ can be found from Eq. (8). After substituting for the magnetic and electric fields, Eqs. (5) and (6), and using Eqs. (2), (14) and (15), we have after some algebra

$$\bar{\mathbf{w}}_x = -\frac{ck_z}{2\mu_0}\left(\mathcal{T} - 2i\alpha\beta^* \mathcal{D}\right)\sin\phi\,|\mathcal{F}|^2, \tag{24}$$

$$\bar{\mathbf{w}}_y = \frac{ck_z}{2\mu_0}\left(\mathcal{T} + 2i\beta\alpha^* \mathcal{D}\right)\cos\phi\,|\mathcal{F}|^2, \tag{25}$$

and

$$\bar{\mathbf{w}}_z = \frac{ck_z^2}{2\mu_0}|\mathcal{F}|^2. \tag{26}$$

The linear momentum density vector $\bar{\pi}$ is related to the Poynitng vector $\bar{\mathbf{w}}$, as defined in Eq. (9). Thus, Eqs. (24) to (26) are used to evaluate the total AM, given by Eq. (10). The components of the cycle-averaged AM density vector $\bar{j}$ can be all evaluated in the focal plane $z = 0$ as follows

$$\bar{j}_x = \frac{\bar{\mathbf{w}}_z}{c^2}\rho\sin\phi = \frac{ck_z^2}{2\mu_0 c^2}|\mathcal{F}|^2\rho\sin\phi, \tag{27}$$

$$\bar{j}_y = -\frac{\bar{\mathbf{w}}_z}{c^2}\rho\cos\phi = -\frac{ck_z^2}{2\mu_0 c^2}|\mathcal{F}|^2\rho\cos\phi, \tag{28}$$

and

$$\bar{j}_z = \frac{1}{c^2}\left(\rho\cos\phi\bar{\mathbf{w}}_y - \rho\sin\phi\bar{\mathbf{w}}_x\right) = \frac{ck_z}{2\mu_0 c^2}\left(\ell - \rho\sigma\mathcal{D}\right)|\mathcal{F}|^2. \tag{29}$$

Since an integration of $\cos\phi$ and of $\sin\phi$ from 0 to 2π gives a result equal to zero, the x- and y- components of $\bar{j}$ are zero similar to the case of the transverse components of the SAM density. Although both transverse components of the SAM and the AM vanish on integration, their density distributions are considered to lead to different areas of applications, such as optical chirality in the interaction with chiral matter, optical sensing of biosystems, near-field microscopy, plasmonic devices, and the manipulation of atoms and molecules, as well as the control of bulk matter at the nanoscale [17,18].

The only non-vanishing AM component is the z-component. Substituting for $\mathcal{D}$ from Eq. (16), with $\mathcal{F}$ from Eq. (3), we obtain

$$\bar{J}_z = \frac{\mathcal{E}_0^2}{\omega^2}\frac{\pi c k_z}{\mu_0 c^2}\int_0^\infty \left\{\ell - \rho\sigma\left(-\frac{2\rho}{w_0^2} + \frac{|\ell|}{\rho} - k_\perp \frac{J_{|\ell|+1}\left(k_\perp\rho\right)}{J_{|\ell|}\left(k_\perp\rho\right)}\right)\right\}\left|J_{|\ell|}\left(k_\perp\rho\right)\right|^2 e^{-\frac{2\rho^2}{w_0^2}}\rho d\rho. \tag{30}$$

The details of the integrals are shown in Appendix B. We have

$$\bar{J}_z = \frac{\mathcal{E}_0^2}{\omega^2}\frac{\pi c k_z}{\mu_0 c^2}\left[\ell I_1 - \sigma\left(I_2 + I_3 + I_4\right)\right] = \frac{\mathcal{E}_0^2}{\omega^2}\frac{\pi c k_z w_0^2}{4\mu_0 c^2} I_{|\ell|}\left(\frac{k_\perp^2 w_0^2}{4}\right) e^{-\frac{k_\perp^2 w_0^2}{4}}\left(\ell + \sigma\right). \tag{31}$$

Substituting for $\mathcal{E}_0$, we obtain

$$\bar{J}_z = \frac{\mathcal{P}}{c^2 k_z}\left(\ell + \sigma\right) = \widetilde{L}\left(\ell + \sigma\right), \tag{32}$$

where $\widetilde{L}$ is a constant that has the dimensions of angular momentum per unit length.

The cycle-averaged energy density can be obtained by multiplying the longitudinal component of the linear momentum density $\bar{\pi}_z$ by the light velocity c, so we have the integral

$$\bar{U} = \int_0^{2\pi} d\phi \int_0^\infty c\left(\frac{\bar{\mathbf{w}}_z}{c^2}\right)\rho d\rho. \tag{33}$$

Using Eq. (26), we have

$$\bar{U} = \frac{\pi k_z^2 \mathcal{E}_0^2}{\mu_0 \omega^2}\int_0^\infty \left|J_{|\ell|}\left(k_\perp\rho\right)\right|^2 e^{-\frac{2\rho^2}{w_0^2}}\rho d\rho, \tag{34}$$

which gives

$$\bar{U} = \frac{\pi k_z^2 \mathcal{E}_0^2}{\mu_0 \omega^2}\frac{w_0^2}{4} e^{-\frac{k_\perp^2 w_0^2}{4}} I_{|\ell|}\left(\frac{k_\perp^2 w_0^2}{4}\right) = \frac{\mathcal{P}}{c}, \tag{35}$$

where we have substituted for $\mathcal{E}_0$ from Eq. (4). It is straightforward to check that it has the dimensions of energy per unit length.

The ratio of the total AM per unit length and energy per unit length follows directly from Eq. (32) and (35)

$$\frac{\bar{J}_z}{\bar{U}} = \frac{\left(\ell + \sigma\right)\mathcal{P}/\left(c^2 k_z\right)}{\mathcal{P}/c} = \frac{\ell + \sigma}{\omega\sqrt{1 - (k_\perp c/\omega)^2}}, \tag{36}$$

where we have used $k_z = \sqrt{(\omega/c)^2 - k_\perp^2}$. This result agrees with the result for the TOB modes [14], which differs from the standard result obtained by Allen et al. [19]. Here, $k_\perp$ is the argument of the Bessel function, which is associated with the rapidity of the oscillatory variation in the radial distance. According to the square root factor in the denominator of Eq. (36), small values of $k_\perp$ lead to the common result $(\ell + \sigma)/\omega$, while large values of $k_\perp$ will increase the longitudinal AM component.

6. Helicity density of BG beams

The optical helicity is one of the prominent properties associated with optical vortex beams that has been widely studied recently [20–25] with its relation to the SAM [14,15,26–32]. The expression of helicity density $\bar{\eta}$, as defined in Eq. (11), is obtained by using the magnetic and electric fields in Eqs. (5) and (6) to calculate the dot product $\mathbf{E}^* \cdot \mathbf{B}$, which is given by

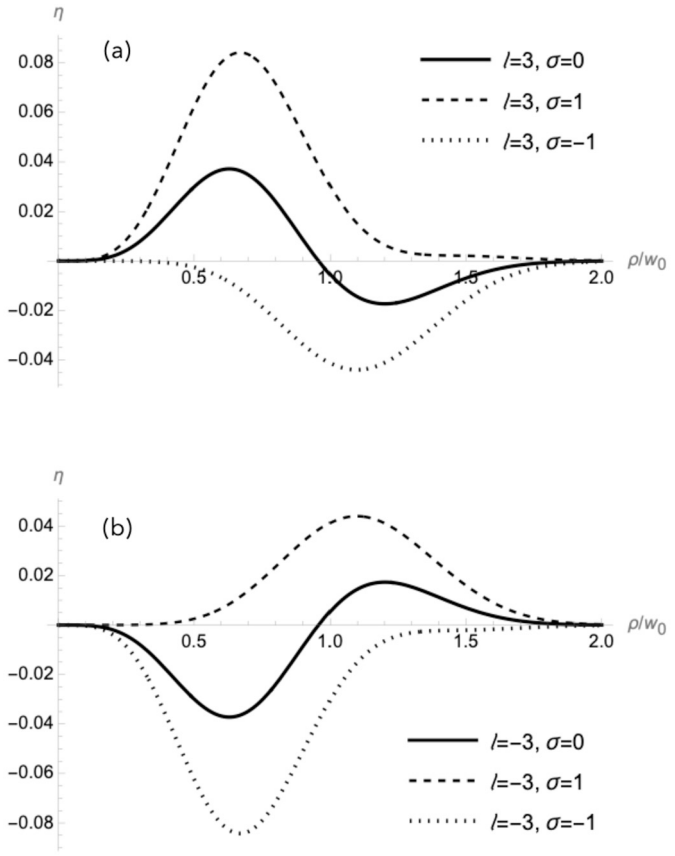

Fig. 1. The helicity density in the focal plane $z = 0$ as a function of the radial variations (in w_0 units) for BG beams of third order for the three cases of polarization in which $\sigma = 0, \pm 1$. (a) For $\ell = 3$ and (b) for $\ell = -3$. We take $k_\perp / w_0 = 3$ and $w_0 = \lambda$, where λ is the beam wavelength.

$$\mathbf{E}^* \cdot \mathbf{B} = c k_z^2 \left(\alpha\beta^* - \beta\alpha^*\right) |\mathcal{F}|^2 - c \left[\beta\alpha^* \left|\frac{\partial \mathcal{F}}{\partial x}\right|^2 - \alpha\beta^* \left|\frac{\partial \mathcal{F}}{\partial y}\right|^2 + |\beta|^2 \left(\frac{\partial \mathcal{F}}{\partial x}\right)\left(\frac{\partial \mathcal{F}}{\partial y}\right)^* - |\alpha|^2 \left(\frac{\partial \mathcal{F}}{\partial x}\right)^* \left(\frac{\partial \mathcal{F}}{\partial y}\right)\right]. \tag{37}$$

Consider the terms that result from the dot product of the first-order longitudinal components of $\mathbf{E}^*$ and $\mathbf{B}$ in Eq. (37)

$$\begin{aligned} E_z^* B_z &= -c \left[\beta\alpha^* \left|\frac{\partial \mathcal{F}}{\partial x}\right|^2 - \alpha\beta^* \left|\frac{\partial \mathcal{F}}{\partial y}\right|^2 + |\beta|^2 \left(\frac{\partial \mathcal{F}}{\partial x}\right)\left(\frac{\partial \mathcal{F}}{\partial y}\right)^* \right. \\ &\quad \left. - |\alpha|^2 \left(\frac{\partial \mathcal{F}}{\partial x}\right)^* \left(\frac{\partial \mathcal{F}}{\partial y}\right)\right] \\ &= -c \left[\frac{i}{2}\sigma \left(\mathcal{D}^2 + \mathcal{T}^2\right) - i\mathcal{D}\mathcal{T}\right] |\mathcal{F}|^2 . \end{aligned} \tag{38}$$

Then, we have for the cycle-average helicity density

$$\bar{\eta}_{\ell\sigma} = \frac{\epsilon_0 c^2}{4\omega} \left[\sigma \left(2k_z^2 + \mathcal{D}^2 + \mathcal{T}^2\right) - 2\mathcal{D}\mathcal{T}\right] |\mathcal{F}|^2 . \tag{39}$$

This expression contains the terms $\left(\mathcal{D}^2 + \mathcal{T}^2\right)|\mathcal{F}|^2$ that arise from the presence of the longitudinal field components and which are proportional to σ in addition to the term that results from the zeroth-order transverse fields. The longitudinal fields are also responsible for the appearance of the last term $-2\mathcal{D}\mathcal{T}\,|\mathcal{F}|^2$. Substituting for $\mathcal{T}$, the helicity density then reads

$$\bar{\eta}_{\ell\sigma} = \frac{\epsilon_0 c^2}{4\omega} \left\{\sigma \left[2k_z^2 + \mathcal{D}^2 + \left(\frac{\ell}{\rho}\right)^2\right] - \ell \left(\frac{2\mathcal{D}}{\rho}\right)\right\} |\mathcal{F}|^2 . \tag{40}$$

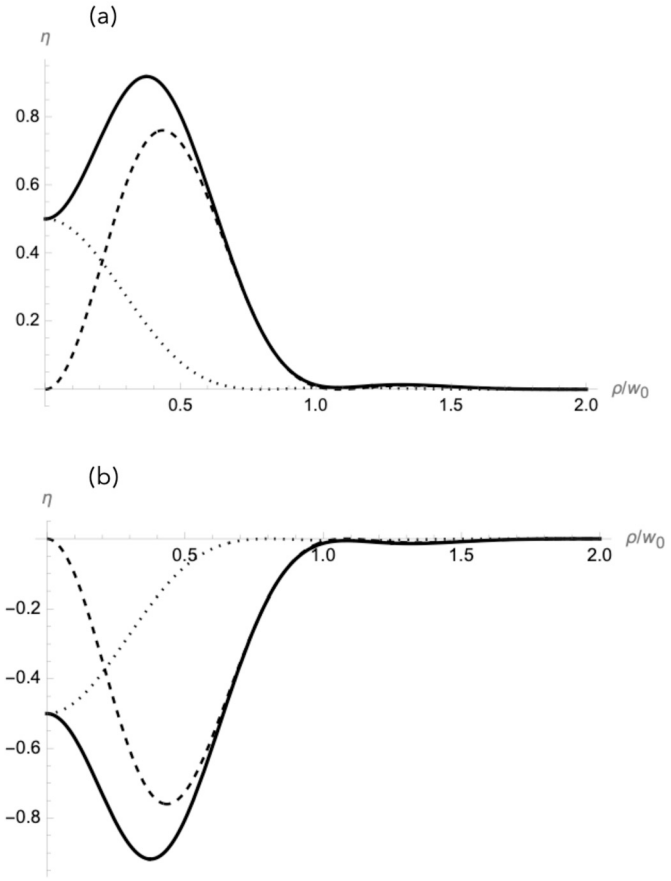

Fig. 2. The helicity density in the focal plane $z = 0$ for circularly-polarized BG beams with $\ell = 0$. (a) For $\sigma = 1$, while (b) for $\sigma = -1$. The dotted curve (dashed curve) represents the transverse (longitudinal) component contributions to the helicity density, and the solid curve is the sum. We take $k_\perp / w_0 = 3$ and $w_0 = \lambda$, where λ is the beam wavelength.

Looking at this equation, we can see that it consists of two parts. In the first part, the density depends on the beam polarization σ and the second part is given by the last term and depends on the winding number ℓ. In Fig. 1, we show the variations of the helicity density for BG beams with different cases of polarization for $\ell = 3$ and $\ell = -3$ in Figs. 1(a) and 1(b), respectively. These plots show that changing the sign of ℓ and/or σ will also change the shape of the helicity density distributions. In this example, we note that $\bar{\eta}_{3,-1}(\rho) = -\bar{\eta}_{-3,1}(\rho)$ and $\bar{\eta}_{3,1}(\rho) = -\bar{\eta}_{-3,-1}(\rho)$.

For a linearly polarized BG beam, i.e., when $\sigma = 0$, the helicity density does not vanish $\bar{\eta}_{\ell 0} \neq 0$. The σ-independent surviving term is due to the purely longitudinal fields. In addition, the helicity density changes its sign when the sign of ℓ changes, such that $\bar{\eta}_{|\ell|0}(\rho) = -\bar{\eta}_{-|\ell|0}(\rho)$. This can be seen by the solid curves in Figs. 1(a) and 1(b).

The helicity density of a BG beam with $\ell = 0$, which is equivalent to the conventional Gaussian beam, is zero for the linearly polarized beam ($\sigma = 0$) and non-zero for the circularly polarized beams ($\sigma = \pm 1$). Thus, the sign of the helicity density in this case depends on the handedness of the circular polarization. The variations of the helicity density for $\sigma = \pm 1$ are shown in Fig. 2 and Fig. 3. Unlike the distributions of the optical helicity due to the transverse fields, which have a Gaussian-shaped profile, the distributions of the longitudinal component contribution take a doughnut shape. Recent work has proposed a direct measurement of the optical chirality of tightly focused Gaussian beams [33], and a study on this has been reported [34].

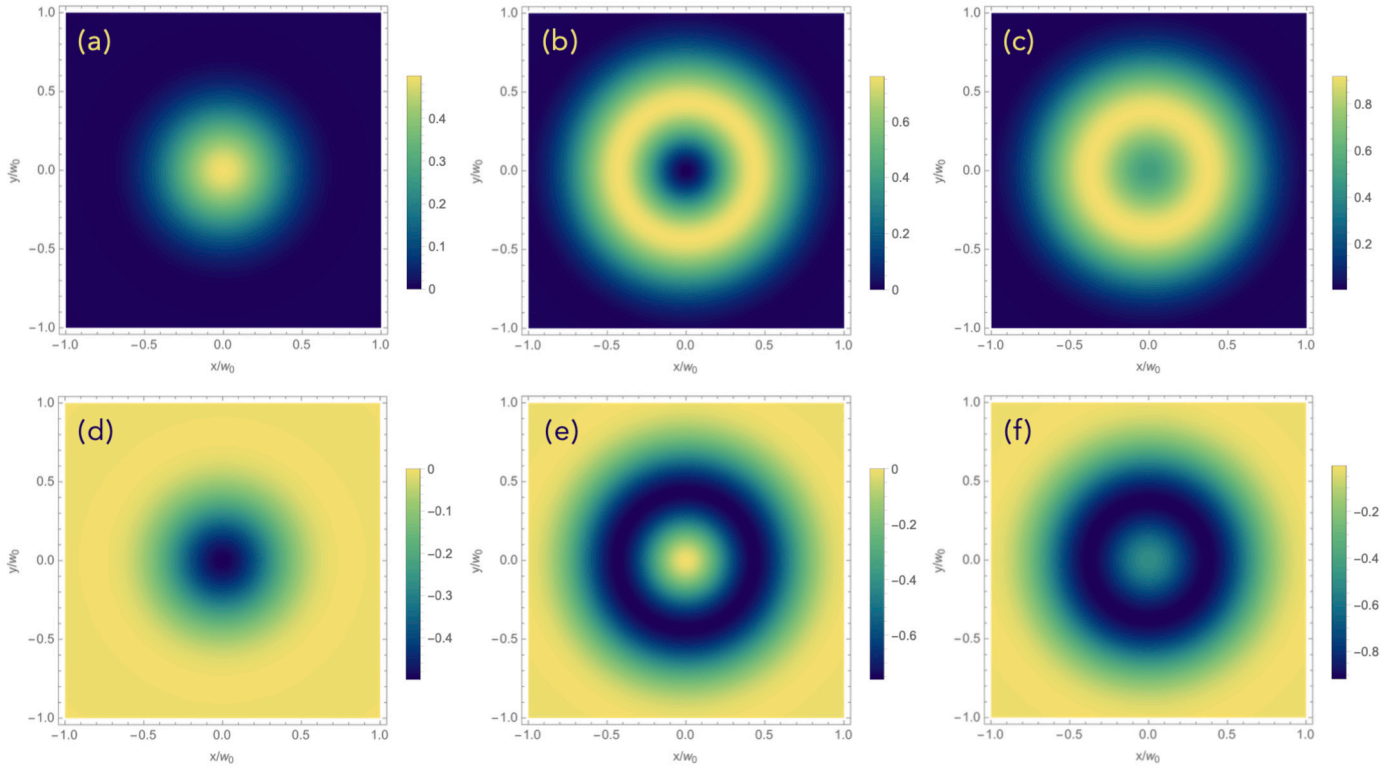

Fig. 3. The in-plane helicity density in the focal plane $z = 0$ for circularly-polarized BG beams with $\ell = 0$. From (a) to (c) with $\sigma = 1$, while from (d) to (f) with $\sigma = -1$. (a) and (d) represent the transverse component, while (b) and (e) represent the longitudinal component contributions to the helicity density. (c) and (f) is the sum. We take $k_\perp/w_0 = 3$ and $w_0 = \lambda$, where λ is the beam wavelength.

7. Integrated helicity

We first consider the total helicity for a linearly polarized BG beam ($\sigma = 0$) which is obtained by integrating over the xy plane. We have

$$\bar{C}_{\ell 0} = \int_0^{2\pi} d\phi \int_0^{\infty} \bar{\eta}_{\ell 0}\, \rho d\rho = 0. \tag{41}$$

The full steps leading to this result are stated in Appendix C. Eq. (41) infers that although the helicity density of a linearly polarized BG mode is non-zero, and which acquires a chiral character [35], its spatial integration vanishes. The non-zero helicity density distributions for linearly polarized BG modes are shown by the solid curves in Figs. 1(a) and 1(b) for two different signs of ℓ. The radial integrations of the density distribution of the areas above and below the optical axis in these figures are zero. Thus, the total helicity is significant only when the optical spin is present and this confirms that OAM alone cannot contribute to the space integral of the helicity density. This result has also been pointed out for both TOB and LG modes in recent published studies [14,15].

The total helicity for circularly polarized BG modes, on the other hand, for which $\sigma \neq 0$ over $\bar{\eta}_{\ell\sigma}$ given in Eq. (40) is given by

$$\bar{C}_{\ell\sigma} = \frac{\epsilon_0 c^2}{4\omega} \int_0^{2\pi} d\phi \int_0^{\infty} \left\{ \sigma \left[2k_z^2 + \mathcal{D}^2 + \left(\frac{\ell}{\rho}\right)^2 \right] - \ell \left(\frac{2\mathcal{D}}{\rho}\right) \right\} |\mathcal{F}|^2 \, \rho d\rho. \tag{42}$$

We can drop the last term in Eq. (42) since it gives zero, as shown in Eq. (41), so

$$\bar{C}_{\ell\sigma} = \frac{\pi \epsilon_0 c^2 \sigma}{2\omega} \int_0^{\infty} \left[2k_z^2 + \mathcal{D}^2 + \left(\frac{\ell}{\rho}\right)^2 \right] |\mathcal{F}|^2 \, \rho d\rho. \tag{43}$$

We can write

$$\bar{C}_{\ell\sigma} = \mathcal{E}_0^2 \frac{\pi \epsilon_0 c^2 \sigma}{2\omega^3} \left(I_1 + I_2 + I_3 \right), \tag{44}$$

where the integrals I_1, I_2 and I_3 are respectively, the first, second and third integrals in Eq. (43). These integrals are detailed in Appendix D. After substituting the results of the integrals, we find

$$\bar{C}_{\ell\sigma} = \sigma L_0 \left\{ 1 + \frac{(|\ell| + 1)}{k_z^2 w_0^2} + \frac{k_\perp^2}{2k_z^2} \right\}, \tag{45}$$

where we have substituted for $\mathcal{E}_0$ using Eq. (4), and we have the same factor L_0. The first term (unity) in the brackets in Eq. (45) represents the total helicity associated with the transverse fields, while the second and third terms appear as a result of the inclusion of the longitudinal-field terms. The magnitude of these terms depends on the degree of focusing as well as the magnitude of ℓ. The second term becomes comparable to unity for strongly focused beams for which the value of w_0 is small or for a very large value of ℓ for moderate focusing, while the ratio $k_\perp^2/2k_z^2$ of the third term becomes significant only when the strength of the focus increases. For the case $w_0 \to \infty$, the second and third terms vanish when we consider the field is weakly focused, and the total helicity reduces to $\bar{C}_{\ell\sigma} = \sigma L_0$, which is simply the helicity of an ideal Bessel beam. By multiplying and dividing the third term by w_0, the second and third terms can equal or exceed unity for values of w_0 given by

$$w_0 \leq \bar{\lambda} \sqrt{\frac{|\ell| + 1}{1 - \left(k_\perp^2/2k_z^2\right)}}, \tag{46}$$

where $\bar{\lambda} = \lambda/2\pi$ is the reduced wavelength. This condition emphasizes that the second and third terms become important relative to unity for a circularly polarized BG beam under tight focusing. For a mode with $\ell = 0$ and $k_\perp = 0$ (a Gaussian mode), we have

$$\bar{C}_{0\sigma} = \sigma L_0 \left\{ 1 + \frac{1}{k_z^2 w_0^2} \right\}, \tag{47}$$

which coincides with the result in Ref. [15]. Note that in this case, the second term equals to unity when $w_0 = \bar{\lambda}$.

8. Conclusions

In this work, we have studied the main optical properties of BG beams in the plane $z = 0$, namely spin, angular momentum, energy, helicity density and the total helicity. Modes of BG type modulate the transverse field distributions of the Bessel beams by a Gaussian profile and are thus termed Bessel-Gaussian beams. We must point out that our calculations follow the methods developed in the works [14,15] but here we apply them for the case of a BG, something that has not been done before. In the limiting cases where a BG approaches a TOB or a Bessel beam, these are recovered in this work. In our work, all beam properties are presented together (both local and averaged over the focal plane). Moreover, in contrast to other works in our formalism the expressions are given in physical units, preserving the dimensional constants (c, ω, ϵ_0, and μ_0), which are not written down in many articles on optical topics.

Similar to the TOB modes [14], we have obtained, for the BG modes, the same ratio of the total AM to the energy per unit length, which does not coincide with the one that displayed by Allen et al. [19]. It differs by a square-root factor in the denominator, which is dependent on the parameter $k_\perp$. This result could be amenable to experimental verification.

We have highlighted similar results as those obtained for other types of modes, namely TOB modes and LG modes [14,15]. One of these results, which was observed also for TOB and LG beams, is the vanishing of the total helicity for linearly polarized BG beams, even though the helicity density expression with $\sigma = 0$ has a non-vanishing ℓ-dependent term due to the contribution of the fully longitudinal components. This term exhibits a chiral behavior in the sense that the sign of the helicity density is affected by the handedness of ℓ. However, the magnitude of the longitudinal components is comparable to the transverse ones only when the beam size is comparable with the optical wavelength.

We have also examined the total helicity for the case of circularly polarized BG beams when $\sigma = \pm 1$. The result in Eq. (45) includes the two terms $(|\ell| + 1)/k_z^2 w_0^2 + k_\perp^2/2k_z^2$ which vanish for a free Bessel beam, and thus the total helicity becomes $\bar{C}_{\ell\sigma} = \sigma L_0$. These two terms result from taking the longitudinal fields into account.

This study has concern on taking the electric and magnetic fields up to the first-order. Higher-order terms of both **E** and **B** are smaller than the zeroth-order and the first-order terms in magnitude and are normally ignored. They can be obtained using Maxwell's equations in an iterative analytical method. The calculations presented here can be extended up to the second-order to see whether these terms affect the optical properties or not.

CRediT authorship contribution statement

M. Alquraishi: Writing – original draft, Resources, Investigation, Formal analysis, Conceptualization. **V.E. Lembessis:** Validation, Supervision, Conceptualization.

Declaration of competing interest

The authors declare that they have no known competing financial interests or personal relationships that could have appeared to influence the work reported in this paper.

Acknowledgement

The authors would like to thank Professor M. Babiker for his comments on the manuscript.

Appendix A. The normalization factor $\mathcal{E}_0$

The overall normalization factor that appears in the form of the BG beam is related to the applied power $\mathcal{P}$, which is the space integral of the z-component of the Poynting vector $(\mathbf{E}^* \times \mathbf{B})/2\mu_0$ over the beam cross-section for which the surface element is $\mathbf{d\Sigma} = d\Sigma \hat{\mathbf{z}}$, thus, the only component of the Poynting vector that enters the integration is the z-component. We have

$$\mathcal{P} = \frac{1}{2\mu_0} \int_0^{2\pi} d\phi \int_0^{\infty} \left| \left(\mathbf{E}^* \times \mathbf{B} \right)_z \right| \rho d\rho, \tag{A.1}$$

with

$$\left| \left(\mathbf{E}^* \times \mathbf{B} \right)_z \right| = c k_z^2 \left| \mathcal{F} \right|^2. \tag{A.2}$$

Substituting for $|\mathcal{F}|^2$, we have

$$\mathcal{P} = \frac{\mathcal{E}_0^2}{\omega^2} \left(\frac{\pi c k_z^2}{\mu_0} \right) \int_0^{\infty} \left| J_{|\ell|} \left(k_\perp \rho \right) \right|^2 e^{-\frac{2\rho^2}{w_0^2}} \rho d\rho. \tag{A.3}$$

We then make use of the standard integral

$$\begin{aligned} &\int_0^{\infty} \left| J_{|\ell|} \left(k_\perp \rho \right) \right|^2 e^{-\frac{2\rho^2}{w_0^2}} \rho d\rho \\ &= \frac{w_0^2}{4} e^{-\frac{k_\perp^2 w_0^2}{4}} I_{|\ell|} \left(\frac{k_\perp^2 w_0^2}{4} \right). \end{aligned} \tag{A.4}$$

Here $I_{|\ell|}$ is the modified Bessel function of the first kind of order ℓ. We, therefore, write

$$\mathcal{P} = \frac{\mathcal{E}_0^2}{\omega^2} \left(\frac{\pi c k_z^2}{\mu_0} \right) \frac{w_0^2}{4} e^{-\frac{k_\perp^2 w_0^2}{4}} I_{|\ell|} \left(\frac{k_\perp^2 w_0^2}{4} \right). \tag{A.5}$$

Finally, we obtain for $\mathcal{E}_0$

$$\mathcal{E}_0^2 = \frac{4\mu_0 \mathcal{P} \omega^2}{c\pi k_z^2 w_0^2 e^{-\frac{k_\perp^2 w_0^2}{4}} I_{|\ell|} \left(\frac{k_\perp^2 w_0^2}{4} \right)}. \tag{A.6}$$

Appendix B. Evaluation of Eq. (30)

We have for the first integral I_1 [36]

$$\begin{aligned} I_1 &= \int_0^{\infty} \left| J_{|\ell|} \left(k_\perp \rho \right) \right|^2 e^{-\frac{2\rho^2}{w_0^2}} \rho d\rho \\ &= \frac{w_0^2}{4} e^{-\frac{k_\perp^2 w_0^2}{4}} I_{|\ell|} \left(\frac{k_\perp^2 w_0^2}{4} \right). \end{aligned} \tag{B.1}$$

The integrals I_2, I_3 and I_4, respectively, are given by

$$\begin{aligned} I_2 &= -\frac{2}{w_0^2} \int_0^{\infty} \left| J_{|\ell|} \left(k_\perp \rho \right) \right|^2 e^{-\frac{2\rho^2}{w_0^2}} \rho^3 d\rho \\ &= -\frac{w_0^2}{16} e^{-\frac{k_\perp^2 w_0^2}{4}} \left[k_\perp^2 w_0^2 I_{|\ell|+1} \left(\frac{k_\perp^2 w_0^2}{4} \right) \right. \\ &\left. + \left(4|\ell| + 4 - k_\perp^2 w_0^2 \right) I_{|\ell|} \left(\frac{k_\perp^2 w_0^2}{4} \right) \right], \end{aligned} \tag{B.2}$$

$$I_3 = |\ell| \int_0^\infty \left|J_{|\ell|}\left(k_\perp \rho\right)\right|^2 e^{-\frac{2\rho^2}{w_0^2}} \rho d\rho = \frac{|\ell| w_0^2}{4} e^{-\frac{k_\perp^2 w_0^2}{4}} I_{|\ell|}\left(\frac{k_\perp^2 w_0^2}{4}\right), \tag{B.3}$$

and

$$I_4 = -k_\perp \int_0^\infty J_{|\ell|}\left(k_\perp \rho\right) J_{|\ell|+1}\left(k_\perp \rho\right) e^{-\frac{2\rho^2}{w_0^2}} \rho^2 d\rho = -\frac{k_\perp^2 w_0^4}{16}\left[I_{|\ell|}\left(\frac{k_\perp^2 w_0^2}{4}\right) - I_{|\ell|+1}\left(\frac{k_\perp^2 w_0^2}{4}\right)\right] \times e^{-\frac{k_\perp^2 w_0^2}{4}}. \tag{B.4}$$

The sum of the three above integrals gives

$$I_2 + I_3 + I_4 = -\frac{w_0^2}{4} e^{-\frac{k_\perp^2 w_0^2}{4}} I_{|\ell|}\left(\frac{k_\perp^2 w_0^2}{4}\right). \tag{B.5}$$

Appendix C. Verification of Eq. (41)

Here, we show that the total helicity of the linearly polarized BG beam for which $\sigma = 0$ vanishes for any value of ℓ. Using Eq. (16), the radial integration takes the following form

$$I_\ell = \int_0^\infty \frac{\omega^2}{\mathcal{E}_0^2}\left(\frac{D}{\rho}\right)|\mathcal{F}|^2 \rho d\rho = \int_0^\infty \frac{\omega^2}{\mathcal{E}_0^2}\left\{-\frac{2\rho}{w_0^2} + \frac{|\ell|}{\rho} - k_\perp \frac{J_{|\ell|+1}\left(k_\perp \rho\right)}{J_{|\ell|}\left(k_\perp \rho\right)}\right\}|\mathcal{F}|^2 d\rho. \tag{C.1}$$

Now we have three integrals to deal with. Substituting for $|\mathcal{F}|^2$, we write

$$I_\ell = -\frac{2}{w_0^2}\int_0^\infty \left|J_{|\ell|}\left(k_\perp \rho\right)\right|^2 e^{-\frac{2\rho^2}{w_0^2}} \rho d\rho + |\ell| \int_0^\infty \left|J_{|\ell|}\left(k_\perp \rho\right)\right|^2 e^{-\frac{2\rho^2}{w_0^2}} \frac{1}{\rho} d\rho - k_\perp \int_0^\infty J_{|\ell|+1}\left(k_\perp \rho\right) J_{|\ell|}\left(k_\perp \rho\right) e^{-\frac{2\rho^2}{w_0^2}} d\rho. \tag{C.2}$$

We make use of the following identity to combine the last two integrals into one integral

$$\frac{d}{dx} J_{|\ell|}(x) = \frac{|\ell|}{x} J_{|\ell|}(x) - J_{|\ell|+1}(x), \tag{C.3}$$

where $x = k_\perp \rho$, and which yields

$$I_\ell = -\frac{2}{w_0^2}\int_0^\infty \left|J_{|\ell|}\left(k_\perp \rho\right)\right|^2 e^{-\frac{2\rho^2}{w_0^2}} \rho d\rho + \frac{1}{2}\int_0^\infty \frac{d}{d\rho}\left|J_{|\ell|}\left(k_\perp \rho\right)\right|^2 e^{-\frac{2\rho^2}{w_0^2}} d\rho. \tag{C.4}$$

The last integral can be integrated by parts, so we have

$$I_\ell = -\frac{2}{w_0^2}\int_0^\infty \left|J_{|\ell|}\left(k_\perp \rho\right)\right|^2 e^{-\frac{2\rho^2}{w_0^2}} \rho d\rho + \frac{1}{2}\left|J_{|\ell|}\left(k_\perp \rho\right)\right|^2 e^{-\frac{2\rho^2}{w_0^2}}\Big|_0^\infty + \frac{2}{w_0^2}\int_0^\infty \left|J_{|\ell|}\left(k_\perp \rho\right)\right|^2 e^{-\frac{2\rho^2}{w_0^2}} \rho d\rho = 0. \tag{C.5}$$

The second term is equal to zero at both limits for $|\ell| > 0$. Although at the limit $\rho = 0$ we have $J_0(0) = 1$ for $\ell = 0$, the helicity density itself is zero since it is proportional to ℓ. This leads to the conclusion that the space integral of $\eta_{\ell 0}$ vanishes because of the vanishing radial integral. Thus, we write

$$\bar{C}_{\ell 0} = 0. \tag{C.6}$$

Appendix D. Evaluation of Eq. (44)

The result of the first integral I_1 is:

$$I_1 = 2k_z^2 \int_0^\infty \left|J_{|\ell|}\left(k_\perp \rho\right)\right|^2 e^{-\frac{2\rho^2}{w_0^2}} \rho d\rho = \frac{k_z^2 w_0^2}{2} e^{-\frac{k_\perp^2 w_0^2}{4}} I_{|\ell|}\left(\frac{k_\perp^2 w_0^2}{4}\right). \tag{D.1}$$

The relevant expressions for the second I_2 and the third I_3 integrals are

$$I_2 = \int_0^\infty \left(-\frac{2\rho}{w_0^2} + \frac{|\ell|}{\rho} - k_\perp \frac{J_{|\ell|+1}\left(k_\perp \rho\right)}{J_{|\ell|}\left(k_\perp \rho\right)}\right)^2 \times \left|J_{|\ell|}\left(k_\perp \rho\right)\right|^2 e^{-\frac{2\rho^2}{w_0^2}} \rho d\rho, \tag{D.2}$$

$$I_3 = \ell^2 \int_0^\infty \left|J_{|\ell|}\left(k_\perp \rho\right)\right|^2 e^{-\frac{2\rho^2}{w_0^2}} \frac{1}{\rho} d\rho. \tag{D.3}$$

We deal with the second integral I_2 as follows

$$I_2 = \int_0^\infty \left[\frac{4\rho^2}{w_0^4} + \left(\frac{|\ell|}{\rho}\right)^2 + \left(k_\perp \frac{J_{|\ell|+1}\left(k_\perp \rho\right)}{J_{|\ell|}\left(k_\perp \rho\right)}\right)^2 - \frac{4|\ell|}{w_0^2} + 4k_\perp \frac{\rho}{w_0^2}\frac{J_{|\ell|+1}\left(k_\perp \rho\right)}{J_{|\ell|}\left(k_\perp \rho\right)} - 2k_\perp \frac{|\ell|}{\rho}\frac{J_{|\ell|+1}\left(k_\perp \rho\right)}{J_{|\ell|}\left(k_\perp \rho\right)}\right] \left|J_{|\ell|}\left(k_\perp \rho\right)\right|^2 e^{-\frac{2\rho^2}{w_0^2}} \rho d\rho \tag{D.4}$$

$$= I_4 + I_5 + I_6 + I_7 + I_8 + I_9,$$

where

$$I_4 = \frac{4}{w_0^4}\int_0^\infty \left|J_{|\ell|}\left(k_\perp \rho\right)\right|^2 e^{-\frac{2\rho^2}{w_0^2}} \rho^3 d\rho = \frac{1}{8} e^{-\frac{k_\perp^2 w_0^2}{4}}\left[k_\perp^2 w_0^2 I_{|\ell|+1}\left(\frac{k_\perp^2 w_0^2}{4}\right) + \left(4|\ell| + 4 - k_\perp^2 w_0^2\right) I_{|\ell|}\left(\frac{k_\perp^2 w_0^2}{4}\right)\right], \tag{D.5}$$

$$I_5 = |\ell|^2 \int_0^\infty \left|J_{|\ell|}\left(k_\perp \rho\right)\right|^2 e^{-\frac{2\rho^2}{w_0^2}} \frac{1}{\rho} d\rho, \tag{D.6}$$

$$I_6 = k_\perp^2 \int_0^\infty \left| J_{|\ell|+1}\left(k_\perp \rho\right)\right|^2 e^{-\frac{2\rho^2}{w_0^2}} \rho d\rho = \frac{k_\perp^2 w_0^2}{4} e^{-\frac{k_\perp^2 w_0^2}{4}} I_{|\ell|+1}\left(\frac{k_\perp^2 w_0^2}{4}\right), \tag{D.7}$$

$$I_7 = -\frac{4|\ell|}{w_0^2} \int_0^\infty \left| J_{|\ell|}\left(k_\perp \rho\right)\right|^2 e^{-\frac{2\rho^2}{w_0^2}} \rho d\rho, \tag{D.8}$$

$$I_8 = \frac{4k_\perp}{w_0^2} \int_0^\infty J_{|\ell|}\left(k_\perp \rho\right) J_{|\ell|+1}\left(k_\perp \rho\right) e^{-\frac{2\rho^2}{w_0^2}} \rho^2 d\rho = \frac{k_\perp^2 w_0^2}{4} e^{-\frac{k_\perp^2 w_0^2}{4}} \left[I_{|\ell|}\left(\frac{k_\perp^2 w_0^2}{4}\right) I_{|\ell|+1}\left(\frac{k_\perp^2 w_0^2}{4}\right)\right], \tag{D.9}$$

and

$$I_9 = -2k_\perp |\ell| \int_0^\infty J_{|\ell|}\left(k_\perp \rho\right) J_{|\ell|+1}\left(k_\perp \rho\right) e^{-\frac{2\rho^2}{w_0^2}} d\rho. \tag{D.10}$$

We can make use of the following identity for the I_9 integral

$$\frac{d}{dx} J_{|\ell|}(x) = \frac{|\ell|}{x} J_{|\ell|}(x) - J_{|\ell|+1}(x), \tag{D.11}$$

where $x = k_\perp \rho$. Then we have

$$\begin{aligned} I_9 &= -2|\ell|^2 \int_0^\infty \left| J_{|\ell|}\left(k_\perp \rho\right)\right|^2 e^{-\frac{2\rho^2}{w_0^2}} \frac{1}{\rho} d\rho \\ &+ |\ell| \int_0^\infty \frac{d}{d\rho} \left| J_{|\ell|}\left(k_\perp \rho\right)\right|^2 e^{-\frac{2\rho^2}{w_0^2}} d\rho \\ &= -2|\ell|^2 \int_0^\infty \left| J_{|\ell|}\left(k_\perp \rho\right)\right|^2 e^{-\frac{2\rho^2}{w_0^2}} \frac{1}{\rho} d\rho \\ &+ \frac{4|\ell|}{w_0^2} \int_0^\infty \left| J_{|\ell|}\left(k_\perp \rho\right)\right|^2 e^{-\frac{2\rho^2}{w_0^2}} \rho d\rho, \end{aligned} \tag{D.12}$$

where the second term of the integral I_9 is integrated by parts.

Note that the integrals I_3 and I_5 cancel with the first term of the integral I_9, and the integral I_7 cancels with the second term of integral I_9.

Next, we substitute the results of the integrals into Eq. (D.4) to obtain

$$I_2 = \left\{ \frac{(|\ell|+1)}{2} + \frac{k_\perp^2 w_0^2}{8} \right\} I_{|\ell|}\left(\frac{k_\perp^2 w_0^2}{4}\right) e^{-\frac{2\rho^2}{w_0^2}}. \tag{D.13}$$

Finally, we combine all the three integrals

$$I_1 + I_2 + I_3 = \left\{ \frac{\left(k_z^2 w_0^2 + |\ell| + 1\right)}{2} + \frac{k_\perp^2 w_0^2}{8} \right\} I_{|\ell|}\left(\frac{k_\perp^2 w_0^2}{4}\right) e^{-\frac{k_\perp^2 w_0^2}{4}}. \tag{D.14}$$

Data availability

Data will be made available on request.

References

[1] J. Durnin, Exact solutions for nondiffracting beams. I. The scalar theory, J. Opt. Soc. Am. A 4 (4) (1987) 651–654.

[2] J. Durnin, J.J. Miceli, J.H. Eberly, Diffraction-free beams, Phys. Rev. Lett. 58 (15) (1987) 1499.

[3] J. Durnin, J.H. Eberly, J.J. Miceli Jr., Comparison of Bessel and Gaussian beams, Opt. Lett. 13 (1988) 79.

[4] J. Arlt, V. Garcés-Chávez, W. Sibbett, K. Dholakia, Optical micromanipulation using a Bessel light beam, Opt. Commun. 197 (4–6) (2001) 239–245.

[5] V. Garcés-Chávez, D. McGloin, H. Melville, W. Sibbett, K. Dholakia, Simultaneous micromanipulation in multiple planes using a self-reconstructing light beam, Nature 419 (6903) (2002) 145–147.

[6] K. Volke-Sepulveda, V. Garcés-Chávez, S. Chávez-Cerda, J. Arlt, K. Dholakia, Orbital angular momentum of a high-order Bessel light beam, J. Opt. B, Quantum Semiclass. Opt. 4 (2) (2002) S82.

[7] V. Garcés-Chávez, D. McGloin, M.J. Padgett, W. Dultz, H. Schmitzer, K. Dholakia, Observation of the transfer of the local angular momentum density of a multiringed light beam to an optically trapped particle, Phys. Rev. Lett. 91 (9) (2003) 093602.

[8] M. Duocastella, C. Arnold, Bessel and annular beams for materials processing, Laser Photonics Rev. 6 (5) (2012) 607–621.

[9] S. Khonina, N. Kazanskiy, S. Karpeev, M. Butt, Bessel beam: significance and applications—a progressive review, Micromachines 11 (11) (2020) 997.

[10] F. Gori, G. Guattari, C. Padovani, Bessel-Gauss beams, Opt. Commun. 64 (6) (1987) 491–495.

[11] D. McGloin, K. Dholakia, Bessel beams: diffraction in a new light, Contemp. Phys. 46 (1) (2005) 15–28.

[12] X. Yu, A. Todi, H. Tang, Bessel beam generation using a segmented deformable mirror, Appl. Opt. 57 (16) (2018) 4677–4682.

[13] R. Bowman, N. Muller, X. Zambrana-Puyalto, O. Jedrkiewicz, P.D. Trapani, M.J. Padgett, Efficient generation of Bessel beam arrays by means of an SLM, Eur. Phys. J. Spec. Top. 199 (1) (2011) 159–166.

[14] K. Köksal, M. Babiker, V.E. Lembessis, J. Yuan, Truncated optical Bessel modes, Phys. Rev. A 105 (6) (2022) 063512.

[15] K. Köksal, M. Babiker, V.E. Lembessis, J. Yuan, Hopf index and the helicity of elliptically polarized twisted light, J. Opt. Soc. Am. B 39 (2) (2022) 459–466.

[16] A. Niv, G. Biener, V. Kleiner, E. Hasman, Propagation-invariant vectorial Bessel beams obtained by use of quantized Pancharatnam–Berry phase optical elements, Opt. Lett. 29 (2004) 238.

[17] A. Aiello, N. Lindlein, C. Marquardt, G. Leuchs, Transverse angular momentum and geometric spin Hall effect of light, Phys. Rev. Lett. 103 (2009) 100401.

[18] X. Piao, S. Yu, N. Park, Design of transverse spinning of light with globally unique handedness, Phys. Rev. Lett. 120 (2018) 203901.

[19] L. Allen, M.J. Padgett, M. Babiker, IV the orbital angular momentum of light, Prog. Opt. 39 (1999) 291–372.

[20] A.F. Rañada, A topological theory of the electromagnetic field, Lett. Math. Phys. 18 (1989) 97–106.

[21] A.F. Rañada, J. Trueba, Electromagnetic knots, Phys. Lett. A 202 (1995) 337–342.

[22] A. Ranada, J. Trueba, Ball lightning an electromagnetic knot?, Nature 383 (1996) 32.

[23] R.P. Cameron, S.M. Barnett, A.M. Yao, Optical helicity, optical spin and related quantities in electromagnetic theory, New J. Phys. 14 (2012) 053050.

[24] I. Fernandez-Corbaton, X. Zambrana-Puyalto, G. Molina-Terriza, Helicity and angular momentum: a symmetry-based framework for the study of light-matter interactions, Phys. Rev. A 86 (2012) 042103.

[25] G. Afanasiev, Y.P. Stepanovsky, The helicity of the free electromagnetic field and its physical meaning, Il Nuovo Cimento A 109 (1996) 271–279.

[26] Y. Tang, A.E. Cohen, Optical chirality and its interaction with matter, Phys. Rev. Lett. 104 (2010) 163901.

[27] K.Y. Bliokh, F. Nori, Characterizing optical chirality, Phys. Rev. A 83 (2011) 021803(R).

[28] M.M. Coles, D.L. Andrews, Chirality and angular momentum in optical radiation, Phys. Rev. A 85 (2012) 063810.

[29] F. Crimin, N. Mackinnon, J. Götte, S. Barnett, Optical helicity and chirality: conservation and source, applied sciences, Appl. Sci. 9 (2019) 828.

[30] F. Crimin, N. Mackinnon, J. Götte, S. Barnett, On the conservation of helicity in a chiral medium, J. Opt. 31 (2019) 094003.

[31] S. Nechayev, J.S. Eismann, R. Alaee, E. Karimi, R.W. Boyd, P. Banzer, Kelvin's chirality of optical beams, Phys. Rev. A 103 (2021) L031501.

[32] K.A. Forbes, G.A. Jones, Measures of helicity and chirality of optical vortex beams, J. Opt. 23 (2021) 115401.

[33] A.A. Sifat, F. Capolino, E.O. Potma, Force detection of electromagnetic chirality of tightly focused laser beams, ACS Photonics 9 (2022) 2660–2667.

[34] D. Green, K.A. Forbes, Optical chirality of vortex beams at the nanoscale, Nanoscale 15 (2023) 540–552.

[35] P. Woźniak, I. De Leon, K. Höflich, G. Leuchs, P. Banzer, Interaction of light carrying orbital angular momentum with a chiral dipolar scatterer, Optica 6 (2019) 961–965.

[36] I.S. Gradshteyn, I.M. Ryzhik, A. Jeffrey, Table of Integrals, Series and Products, Academic Press, 2007, p. 707.